Self-organisation of mortal filaments: the role of FtsZ treadmilling in bacterial division ring formation

Christian Vanhille-Campos,[1,2] Kevin D. Whitley,[3] Philipp Radler,[1] Martin Loose,[1] Séamus Holden,[4] and Anđela Šarić[1]

[1] *Institute of Science and Technology Austria, Klosterneuburg, Austria*[*]
[2] *Department of Physics and Astronomy, Institute for the Physics of Living Systems, University College London, London, United Kingdom*
[3] *Centre for Bacterial Cell Biology, Biosciences Institute, Newcastle University, Newcastle upon Tyne, United Kingdom*
[4] *School of Life Sciences, The University of Warwick, Coventry, United Kingdom*

(Dated: May 8, 2023)

Functional protein filaments in the cell commonly treadmill – grow and shrink on opposite ends, driven by energy consumption. Treadmilling causes filaments to seem as if they were moving, even though the individual proteins remain static. Here we investigate the role of treadmilling, implemented as dynamic turnover, in the collective filament self-organisation. On the example of the bacterial FtsZ protein, a highly evolutionary conserved tubulin homologue, we show, in computer simulations and *in vitro* experiment, that treadmilling drives filament nematic ordering by means of dissolving misaligned filaments. We demonstrate that this ordering via local dissolution allows the system to quickly respond to chemical and geometrical biases in the cell, and is necessary for the formation of the bacterial division ring in live *Bacillus subtilis*. We finally use simulations to quantitatively explain the characteristic dynamics of FtsZ division ring formation measured *in vivo*. Beyond FtsZ and cytoskeletal filaments, our study identifies a novel mechanism for nematic ordering via constant birth and death of energy-consuming filaments.

Cytoskeletal filaments are active cellular elements that constantly grow and shrink through addition and removal of subunits. One prominent example of this activity is treadmilling – a process in which protein filaments grow on one end, while the other end shrinks at equal rate. This dynamic behaviour is driven by nucleotide hydrolysis, and results in the filaments seemingly moving, despite the individual filament monomers remaining in one place [1]. The most abundant cytoskeletal filaments, such as actin and microtubules, both exhibit this important feature [2–6].

From a physics point of view, treadmilling has been often modelled as self-motility, where the filament centre of mass moves directionally with a certain velocity to mimic the directional filament growth [7–9]. While this approach might be appropriate to describe single filament dynamics, when it comes to the assembly into higher order dynamic structures, self-propelled models might not be suitable. In particular, unlike self-motile filaments, treadmilling polymers have finite lifetimes, undergoing constant turnover, and have been shown not to exert additive forces when colliding with one another [10]. This is expected to result in important differences in their collective organisation and response to external signals. However, the effects of explicit treadmilling kinetics on collective organisation remain unexplored.

Here we develop the first computational model for interacting treadmilling filaments, accounting for the kinetics of nucleation, growth and shrinkage, to study their collective behaviour. We particularly focus on investigating self-organisation of FtsZ filaments, a highly-evolutionary conserved tubulin homolog [11], widely present in bacteria, and one of the best characterised treadmilling systems in the literature [12–15]. Our model allows us to explore the interplay between polymerisation dynamics and collective filament organisation at the cellular scale, and to directly compare to *in vitro* and *in vivo* experiment. Treadmilling FtsZ filaments self-organise into a dynamic ring [16] at the bacterial midcell (the "Z-ring") that triggers bacterial cell division [17–19]. Treadmilling itself has been shown to be essential for the formation of the division ring in *B. subtilis* [20] but it remains unclear what in the treadmilling process enables filament self-organisation into the Z-ring.

We first show that our model correctly reproduces single-filament treadmilling dynamics collected in new *in vitro* measurements [12], and proposed in previous theoretical kinetic studies [21]. We then

[*] andela.saric@ist.ac.at

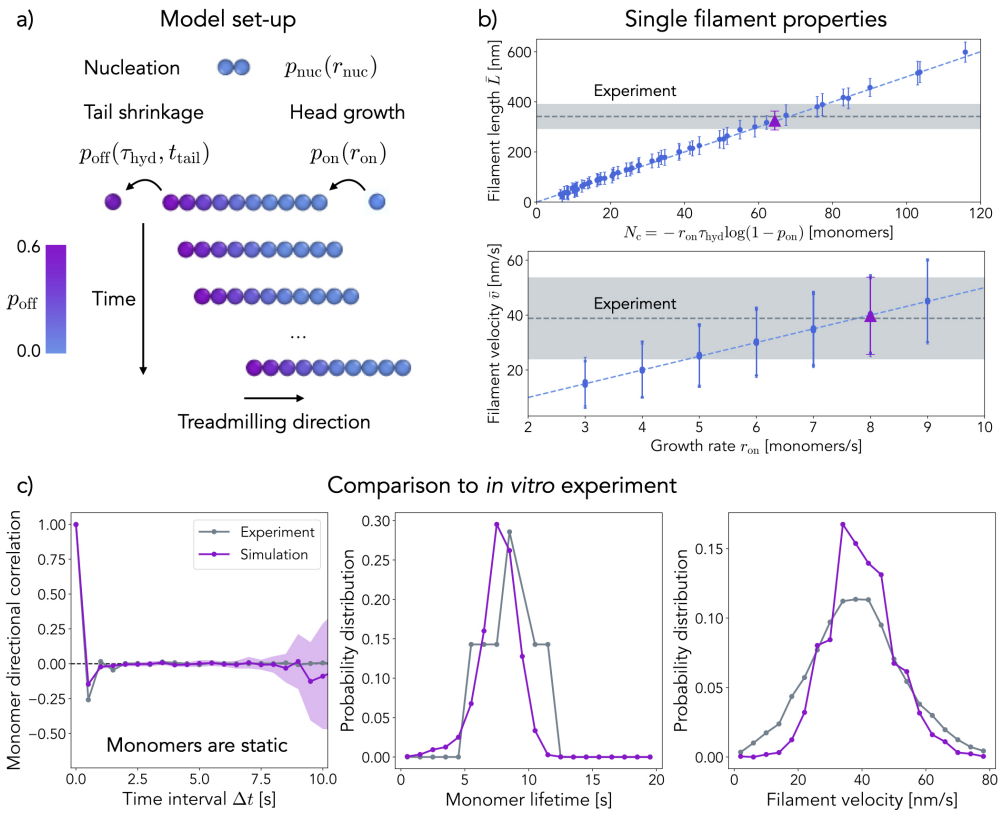

FIG. 1. **Coarse-grained model for treadmilling filaments. a)** New filaments nucleate at a constant rate $r_{\rm nuc}$, grow with probability $p_{on} = r_{\rm on}dt$, and shrink with probability $p_{\rm off}$, determined by the hydrolysis mean time $\tau_{\rm hyd}$ and the time the monomer has been in the system. This growth/shrinkage dynamics results in the apparent directional motion of the filaments over time. **b)** Top panel: Single filament length against the corresponding intrinsic size $N_{\rm c}$. The blue dashed line is the theoretical $\bar{L} = N_{\rm c}\sigma$ ($\sigma = 5$ nm). Bottom panel: Average treadmilling velocity $\bar{v}$ of a filament against the corresponding growth rate $r_{\rm on}$. The blue dashed line is the theoretical $\bar{v} = r_{\rm on}\sigma$. In both panels each point is the steady-state average over 20 replicas with error bars for the standard error of the average. The grey dashed lines correspond to the fluorescence microscopy experiments of *in vitro* reconstituted *E. coli* FtsZ treadmilling filaments on supported lipid bilayers at 1.25μM (shaded areas for error). **c)** Single-filament dynamics in simulations (in purple) quantitatively matches *in vitro* FtsZ dynamics (in grey). Left panel: Directional autocorrelation of FtsZ monomers at increasing time intervals Δt decays quickly, showing the static nature of individual monomers. Middle panel: Treadmilling filament velocity distribution. Right panel: Monomer lifetime distribution. All simulation curves are taken for $r_{\rm on} = 8$ monomers/s and $\tau_{\rm hyd} = 5$ s, which fit experimental measurements best (purple triangles in panel b).

demonstrate that treadmilling polymers collectively align due to shrinkage and "death" of misaligned filaments, yielding quantitative matching with high-speed AFM imaging of reconstituted FtsZ filaments. Finally, we find that such a system forms tight ordered dynamic rings when under external biases present in bacterial division. The model quantitatively explains the time-dependent *in vivo* dynamics of Z-ring condensation and maturation [20, 22] in *B. subtilis*. These results highlight a new model for ordering of cytoskeletal filaments through dynamic growing and shrinking, which is responsible for the formation of the bacterial division ring, and potentially present in a plethora of other cytoskeletal processes across the tree of life.

Model description. We model treadmilling filaments as coarse-grained polymers made of spherical beads with diameter σ (the simulation unit of length) living on a two-dimensional plane with periodic boundary conditions. Individual beads corre-

spond to distinct monomers, such that $\sigma = 5$ nm as measured for FtsZ [18, 23, 24]. Monomers are connected into filaments by harmonic springs and angle potentials to capture filament stiffness (see SI for more details on the model). We impose filament nucleation, growth and shrinkage kinetics via dynamic Monte Carlo (MC) simulations (Figure 1a and Supplementary Movie 1).

Treadmilling filaments are active, dissipating energy via nucleotide hydrolysis at the monomer-monomer interface. This results in a monomer conformational change, which then tends to dissociate when it reaches the tail of the filament [21, 25–27]. To incorporate treadmilling we perform dynamic updates over MC steps of size $dt = 0.1$s where we grow and shrink each individual filament with probabilities p_{on} and p_{off} respectively, and nucleate new filaments with probability p_{nuc}. Treadmilling is controlled with only two parameters: the head polymerisation rate r_{on} and the monomer hydrolysis time τ_{hyd}. Here r_{on} (in monomers/s) captures both the bulk free monomer concentration, which we assume is constant, and the polymerisation rate constant, such that $p_{\mathrm{on}} = r_{\mathrm{on}} dt$. Monomers in solution are thus implicitly considered. Importantly, filament polymerisation is allowed only if free space for monomer addition is available around the filament head. τ_{hyd} corresponds to the hydrolysis mean time (in s), which determines monomer detachment and acts as a timer for tail depolymerisation. For each filament then $p_{\mathrm{off}} = 1 - e^{-t_{\mathrm{tail}}/\tau_{\mathrm{hyd}}}$ where t_{tail} is the time for which the tail monomer has been in the system. To reach steady state $p_{\mathrm{on}} = p_{\mathrm{off}}$ must be satisfied, which defines an intrinsic size $N_{\mathrm{c}} = -r_{\mathrm{on}}\tau_{\mathrm{hyd}} \log(1 - p_{\mathrm{on}})$ around which filaments fluctuate while treadmilling at constant velocity $v_c = r_{\mathrm{on}}\sigma$.

Finally, insertion of new filament nuclei into the system (modelled as dimers) is controlled by the imposed nucleation rate r_{nuc} (in nuclei/s), such that $p_{\mathrm{nuc}} = r_{\mathrm{nuc}} dt$. Like for the growth rate, r_{nuc} captures both the nucleation rate constant and the free monomer concentration.

Single filament dynamics. We first perform simulations of individual filaments for a range of filament growth and monomer hydrolysis parameter sets $\{r_{\mathrm{on}}, \tau_{\mathrm{hyd}}\}$. We initialise the system with a single filament nucleus and let it evolve in time (Supplementary Movie 1). As expected, filaments reach a steady-state where they fluctuate around a constant size and treadmilling velocity (Figure 1b), while the individual monomers display finite lifetimes (Figure S2). Experimentally, FtsZ protofilaments have been measured (*in vivo* and *in vitro*) to be between 100 and 500 nm long and to treadmill at speeds between 15 and 50 nm/s, while individual monomers turnover at lifetimes around 8 seconds, depending on the bacterial strain and conditions [22, 24, 28–30], all of which are well within the range we observe in simulations (Figure 1b).

We now turn to direct comparison of our model with experiment. For this purpose, we reconstituted *E. coli* FtsZ filaments (FtsA and Alexa488-FtsZ) on supported lipid bilayers (SLBs) in a reaction chamber with excess ATP/GTP and used total internal reflection fluorescence (TIRF) microscopy to image treadmilling dynamics (see SI for further details on the experimental setup). Using previously developed image analysis software [31] we measure filament lengths and velocities (grey dashed lines and shaded regions in Figure 1b, also reported in [31]) as well as individual monomer lifetimes (Figure S3). When we choose $\{r_{\mathrm{on}}, \tau_{\mathrm{hyd}}\}$ model parameters that match this specific experimental system (the purple triangles in Figure 1b), the velocity and lifetime distributions also display an excellent agreement with the experimental data (Figure 1c, middle and right panels).

Importantly, the directional autocorrelation function of individual monomers for different time intervals Δt, measured both in simulations and *in vitro* experiments, presents a sharp decay to zero (Figure 1c, left panel), indicating that individual monomers remain static even though the filament as a whole appears to be moving. The same is also clearly visible from the individual molecule track analysis *in vitro* (Figure S5). This lack of motility is an important feature of treadmilling filaments, which also suggests that modelling treadmilling as self-propulsion is likely unsuitable, as individual monomers do not display any directional motion. Consequently, pushing forces exerted by treadmilling filaments are negligible or small, as previously suggested for actin bundles [10]. Together, these results demonstrate that our model correctly captures the main aspects of treadmilling dynamics on biologically relevant time- and length- scales, that it can be benchmarked for a specific protein under particular conditions, and can be used for quantitative comparison with experiment.

Collective filament dynamics. We are now in a unique position to explore the collective dynamics of many treadmilling filaments and how their mortality affects the formation of higher order structures. We nucleate filaments in the system, characterised by parameters $\{r_{\mathrm{on}}, \tau_{\mathrm{hyd}}\}$, at a constant nu-

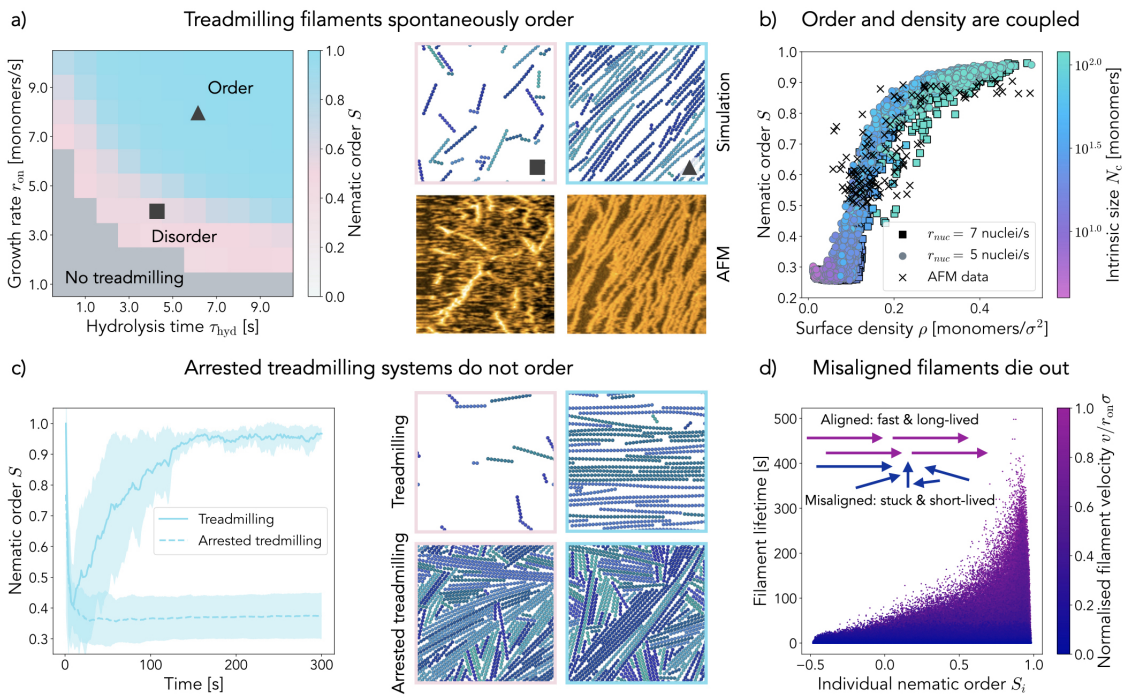

FIG. 2. **Collective behaviour of treadmilling filaments.** **a)** Left: Nematic order parameter S measured in simulations (averaged over 20 replicas). Grey indicates the quasi-empty systems of non-treadmilling filaments, blue the nematically-ordered system with polar bands, and pink the disordered transitional region. Right: Representative simulations snapshots for the two regions (top row; filaments coloured according to their orientation) and AFM images of reconstituted *E. coli* FtsZ on supported lipid bilayers (bottom row). **b)** Coupling between nematic order S and protein surface density ρ in simulations for different kinetic parameters, coloured by the intrinsic filament size N_c. Crosses correspond to S and ρ values computed from the HS-AFM images. **c)** Left: Time evolution of the nematic order parameter S for an ordering system ($r_{on} = 8$ monomers/s, $\tau_{hyd} = 10$ s) showing that the ordering is not achieved when treadmilling is arrested (average over 10 replicas, shaded region is the standard deviation). Right: Representative snapshots of systems in the disordered (left column) and ordered (right column) regions of the parameter space undergoing normal treadmilling kinetics (top row) and arrested treadmilling (bottom row). **d)** Lifetimes of individual filaments against their individual average alignment. Points are coloured according to the average filament treadmilling velocity v scaled by the theoretically expected velocity. The data includes all simulation replicas for highly ordered steady-states ($N_c > 150$, 430 simulations, 1 128 267 filaments in total). Inset: Schematic illustration of the two observed populations of filaments (aligned and misaligned).

cleation rate of r_{nuc}. The system generally reaches steady-state surface density ρ and average filament size $\bar{N}$ even though the filaments population undergoes continuous turnover (Figure S6). We observe three different collective regimes (Figures 2a-b, S7-8), which depend exclusively on the treadmilling kinetics or the resulting intrinsic filament size N_c.

The first regime occurs for very low values of the intrinsic filament size N_c (grey area in Figure 2a), where the individual filaments die out rapidly (Figure S4), resulting in a quasi-zero surface density (see also Figures S7-8). As the intrinsic filament size increases ($N_c \sim 10$) the system transitions into an unstable treadmilling regime, where filament size fluctuations are comparable to their size (Figure S4). The system is populated by viable short-lived treadmilling filaments that stochastically die out, never reaching high surface densities (the pink region in Figure 2a and the corresponding snapshot, Supplementary Movie 2). Finally, for higher values of N_c ($N_c \gg 10$), the intrinsic size fluctuations become negligible compared to the filament size (Figure S4), and filaments enter a highly stable and persistent treadmilling regime in which they can achieve long lifetimes. This allows the system to build up its filament population and reach higher surface densities

(Figures S7-8).

We find that the majority of this parameter space is characterised by the emergence of a large-scale nematic order (Figure 2a-b) and the formation of polar bands (snapshot in Figure 2a and Supplementary Movie 3). This behaviour is highly reminiscent of the *nematic laning* phase previously observed in self-propelled rods [32, 33] and is similarly characterised by high values of local and global nematic order parameter S, and high local but low global values of the polar order parameter P due to lanes formation (Figure S10). Unlike in self-propelled [8, 32, 33] or passive [34, 35] nematic systems, where the system density determines the ordering, in a treadmilling system the filament intrinsic size, a measure of the stability of the kinetics (Figure S4), determines the steady state and the emergent self-organisation (Figures 2b and S8). We find that if monomer hydrolysis, and hence treadmilling, are arrested, such that monomers are "trapped" inside the filaments and the filaments grow long, the system will evolve towards a highly populated but disordered configuration (Figures 2c and S11).

We now turn to comparison of collective ordering with experiment. As shown in Figure 2a, High-Speed Atomic Force Microscopy (HS-AFM) images of *E. coli* FtsZ filaments on a supported bilayer bear a striking resemblance to simulation snapshots, with an evident transition to a high nematic order as the system becomes more populated (Supplementary Movie 4). These high resolution images allow us to quantify both the orientational order and the surface density of the system at any time from vector field analysis (Figure S12), again enabling a quantitative comparison with the simulations. Strikingly, Figure 2b demonstrates that both HS-AFM data and simulation results display the same coupling between orientational order and density, independently of the specific parameters used. These results indicate that the ordering transition unveiled by our modelling approach accurately describes FtsZ treadmilling behaviour as observed experimentally and should therefore provide insight into the mechanisms at play.

The direct matching between simulation and experiment now allows us to identify the mechanism behind the observed self-organisation. We find in simulations that the ordering transition is driven by filaments growing against each other, which eventually selects for a common alignment direction, similarly to systems of self-motile rods [32, 33, 36]. However, the underlying mechanism is completely different: unlike self-motile polymers that exert force when collided with another filament [37–40], treadmilling filaments stop growing when they reach another object, but still continue to depolymerise, which results in shrinkage, reorientation or even dissolution of the filaments (see Supplementary Movie 5). Ultimately, the fact that shrinkage is independent of growth causes misaligned filaments, which are more likely to grow against the neighbours than their aligned counterparts, to die out.

Figure 2d quantifies this "mortal filaments" behaviour by measuring the lifetime of each filament (in an ordered steady-state) against its average alignment, characterised by the individual nematic order S_i. These two variables are indeed highly correlated: only very aligned filaments ($S_i \sim 1$) reach long lifetimes, up to several minutes, while strongly misaligned polymers die out after a few seconds on average and are gradually replaced with aligned ones. The aligned filaments also treadmill with a velocity that approaches their single-filament value $v_c = r_{on}\sigma$, while the misaligned filaments typically have vanishing velocities (colour coded in Figure 2d). Globally this behaviour results in the progressive selection of the more stable filaments that align with the rest of the system, reminiscent of what was previously proposed for plant microtubules [41, 42]. The filament death and replacement mechanism, and the establishment of order, are not rapid, but require turnover of a large number of filaments and typically take minutes (Figure S9).

Treadmilling drives bacterial division ring condensation. We finally investigate the role of treadmilling in live bacterial cells. Our *in vivo* experiments recently showed that treadmilling dynamics of FtsZ is essential for Z-ring formation in division of *B. subtilis* [20], but the mechanism underlying this process remains elusive. We now apply the coarse-grained molecular model for treadmilling filaments to address this question. Bacterial FtsZ has been observed to display mild natural curvature in live cells and *in vitro*, with diameters similar or smaller to typical cell diameters [12, 43–45]. There is however stronger evidence that its main binding partner FtsA – which forms composite polymers with FtsZ, anchoring it to the cell envelope – is intrinsically curved and displays a preference for high membrane curvatures [46]. This suggests that the interplay between cell geometry and curvature of the (composite) filament should favour filament alignment along the circumference of the cell, similarly to what has been previously shown for MreB filaments [47–49]. We incorporate this curvature-sensing mechanism in the model, as shown in Figure

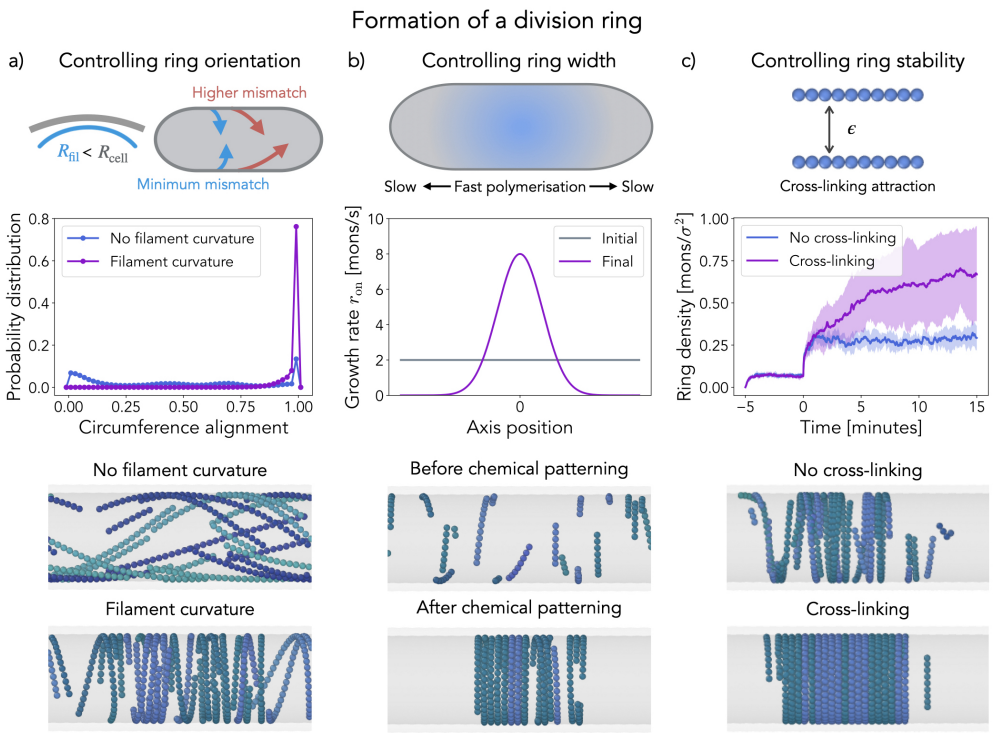

FIG. 3. **Formation of the bacterial division ring. a)** Filament curvature and cell geometry drive the collective filament orientation along the cell circumference. Top panel: Illustration of the curvature-sensing mechanism of FtsZ/FtsA filaments. Middle panel: Distribution of filament orientations with and without filament curvature. Each curve corresponds to the average over 30 simulations at 6 different parameter combinations in the nematic order region of the parameter space. Bottom panel: Two representative snapshots of steady-state configurations of treadmilling filaments with and without filament curvature. **b)** Spatial modulation of FtsZ's growth and nucleation kinetics mediates its midcell localisation. Top panel: Illustration of the typical FtsZ kinetics modulation observed *in vivo*. Middle panel: Example of a kinetics modulation combining an increase in the growth and nucleation rates around the midcell with a decrease at the poles. Bottom panel: Two representative snapshots of system configurations before and after the modulation of the kinetics is switched on. **c)** Attractive interactions stabilise the ring and mediate tight packing. Top panel: illustration of the cross-linking implementation. Middle panel: Ring density in time with and without cross-linking interactions. Bottom panel: Two representative snapshots of steady-state rings with and without cross-linking interactions. In all snapshots the filaments are coloured according to the treadmilling direction.

3a, by considering the energy difference between the filament's intrinsic curvature and the local curvature on the cell (we generally assume $R_{\text{cell}} = 500$ nm and $R_{\text{fil}} = 100$ nm, see SI for details). We find that this energy consideration is sufficient to determine the global orientation of the filaments along the cell circumference (Figure 3a). These results point to the importance of the interplay between filament and cellular geometry in supra-molecular organisation.

Bacteria have evolved a number of different molecular tools that act in complementary ways to position FtsZ filaments to the right division site – the midcell – at the right time. Such systems include dynamic chemical patterning [50–55], condensate formation [56] or chromosome association [57–60] and generally have the effect of spatially modulating the FtsZ treadmilling kinetics, resulting in higher polymerisation rates around the midcell and lower ones around the poles (schematic in Figure 3b). Our model can incorporate this FtsZ growth modulation as an instantaneous change from a case in which the filament growth and nucleation rates are equal along the cell body to a Gaussian shaped modulation of the growth and nucleation rates centered around the midcell, with a constant hydrolysis time (Figure 3b). We find that the resulting combination of the midcell enrichment and cell pole depletion of FtsZ proteins reliably localises the filaments to the midcell region

(Figure 3b) and best captures Z-ring condensation (SI, Figures S14-15).

Finally, we consider one more model ingredient. It has been shown that FtsZ filament cross-linking by FtsZ-binding proteins is required for Z-ring condensation [22, 31, 61]. In line with this, we find that including explicit attractive interactions between filaments has an important stabilising effect on the ring structure, further promoting filament alignment and tight packing, and allowing for a sustained monomer accumulation in the ring over time (Figures 3c and S13). Taken together, these results show that treadmilling filaments in our model can spontaneously form stable ring-like structures when a combination of filament curvature, attractive inter-filament interactions, and spatio-temporal modulation of the filament kinetics are considered.

Comparison with *in vivo* data. We are now in a good position to compare our model for Z-ring formation with live cell data. We have previously found that Z-ring formation in *B. subtilis* has a very particular dynamics *in vivo*: localisation of the ring to the midcell, often referred to as ring condensation, occurs very rapidly, within 1 minute (Figure 4a), while ring maturation via growth and thickening occurs over several minutes (Figure 4b). If treadmilling is impaired early on, the Z-ring cannot form and remains diffuse, while impairing treadmilling during maturation disrupts proper division [20]. Interestingly, our experiment also found that the average velocity of mature Z-rings is substantially faster than that of nascent ones (Figure 4c).

We explore whether our model can capture the dynamics of Z-ring formation *in vivo*, and explain the mechanism behind it. As shown in Figure 4a, our model also displays rapid ring condensation for a wide range of kinetic parameters (Figure S15), which occurs only a few seconds after the switch of the growth rate modulation profile. The reason for this is that the filaments in the growth-inhibited areas of the cell rapidly die out, as their depolymerisation rate is faster than the polymerisation rate. The whole process occurs on the scale of the single monomers lifetime, as controlled by τ_{hyd}.

We further find, in agreement with what has been observed in live cell experiment, that after rapid ring condensation at the site of division, treadmilling filaments in the model accumulate rather slowly, over a time-span of several minutes. The simulations reveal a steadily increasing surface density of monomers in the midcell region that matches well the experimental measurements (Figure 4b). This feature is the inherent result of treadmilling-driven alignment: the ring structure transitions from an initially disordered state to an ordered and tightly-packed state (Figure 4d) through the dissolution and replacement of misaligned filaments. This process is analogous to what we had also observed *in vitro* for *E. coli* FtsZ.

The replacement of misaligned filaments is at heart a trial-and-error process, rendering the ring maturation slow. The decrease in the fraction of low-velocity, misaligned filaments in the mature ring also naturally leads to faster treadmilling velocities without individual filaments speeding up, which matches what has been measured in live cells (Figure 4c). In other words, the filaments that survive all run parallel to each other with treadmilling velocities close to maximal values. Finally, we found that arresting treadmilling in our model has similar effects to those observed *in vivo*. If treadmilling is arrested early on, before the onset of the chemical patterning, the filament population remains diffuse and never condenses to the midcell (Figure 4e). If treadmilling is arrested after the switch of the chemical patterning, the ring forms at the midcell, but displays aberrant, "frozen", configurations (Figures 4e and Figure S18).

Altogether, our treadmilling model naturally reproduces the key dynamical aspects of Z-ring formation observed in live cells. The FtsZ filaments are able to localise to the midcell on timescales similar to the monomer lifetimes, driven by the underlying spatial modulation of the polymerisation rates, while the tightly-packed division rings grow on substantially longer timescales by the virtue of misaligned filaments dying and growing again until only the aligned ones remain (Supplementary Movie 6). More generally, our model explains the importance of treadmilling – dynamic growth and shrinkage of filaments – in localising and timing bacterial division.

Discussion Here we developed a coarse-grained molecular model for explicitly treadmilling filaments in two dimensions, using a polymerisation kinetics that depends on two parameters only: the imposed growth rate r_{on} and the average hydrolysis time τ_{hyd}. Such polymers can grow and shrink on opposite ends at equal rates, virtually displaying directional motion while individual monomers remain static and undergo turnover. By tuning these two parameters the model can replicate experimentally observed FtsZ properties quantitatively, such as the filament lengths and treadmilling velocities, as well as the monomer lifetimes of treadmilling *E. coli* on supported bilayers. Since the model can capture a wide range of filament sizes and velocities by tuning the two parameters, it is also expected to be well-

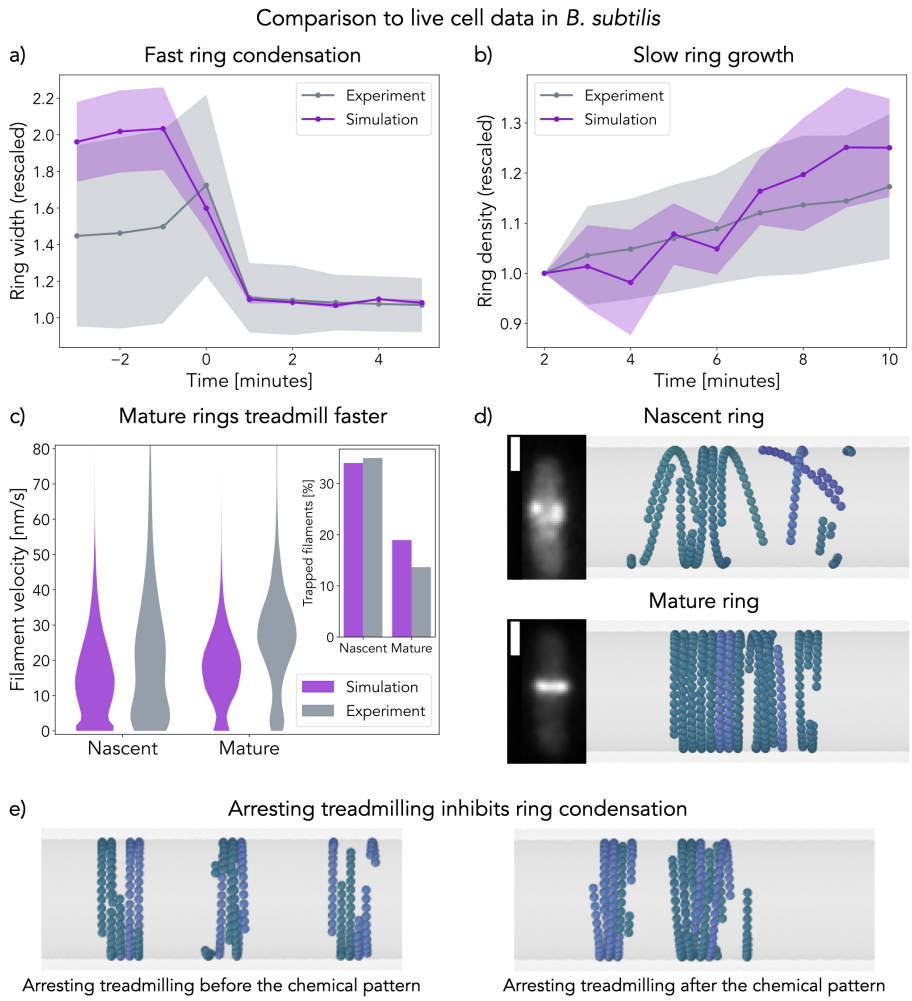

FIG. 4. **Z-ring formation *in vivo*. a)** Z-ring condensation dynamics for live cells (grey) and simulations (purple). A rapid ring collapse around $t = 0$ minutes is observed. **b)** Ring density in time for live cells (grey) and simulations (purple). A positive average slope is observed, indicating the slow accumulation of proteins to the division site. **c)** Filament velocity distributions in nascent and mature rings for live cells (grey) and simulations (purple). Inset: Fraction of stuck filaments ($v < 10$ nm/s) for each distribution. In simulations we define $t < 2$ minutes for nascent and $t > 8$ minutes for mature rings. **d)** Representative snapshots of two successive ring configurations observed *in vivo* and in simulations. Filaments in simulations are coloured according to their orientation with respect to the cell circumference. Microscopy images show fluorescently tagged FtsZ in live *B. subtilis* cells, scale bar is 1μm. **e)** Representative snapshots of systems at $t = 10$ minutes after arresting treadmilling. Treadmilling is arrested 5 minutes before (left panel) and 5 minutes after (right panel) the onset of the chemical pattern that modulates the growth kinetics. The simulation data in panels a), b) and c) corresponds to a switch $r_{\mathrm{on}} = 2 \rightarrow 9$ monomers/s for $\tau_{\mathrm{hyd}} = 15$ seconds and $w_{\mathrm{prof}} = \{80, 100\}$ nm. In panels a) and b) the shaded regions correspond to the standard deviation between parameter sets. Time $t = 0$ corresponds to the onset of the chemical pattern. Note that simulation snapshots are not to cellular scale.

suited to study different cytoskeletal treadmilling proteins.

From a physics point of view, the explicit molecular nature of the model allowed us to flesh out a previously underappreciated or unrecognised mechanism behind self-organisation of treadmilling filaments – the nematic ordering via death of locally misaligned filaments. Our findings are experimentally confirmed by High-Speed AFM imaging of reconstituted FtsZ filaments which display the same

ordering transition, while the individual monomers undergo turnover. The ordering transition, which shows quantitative matching between simulations and experiment, is completely controlled by the kinetics of this out-of-equilibrium system.

Our treadmilling model unveils a surprisingly rich collective behaviour arising from the dissolution and replacement of stuck filaments, which is characteristic of mortal polymers. These findings put forward treadmilling filaments as a paradigm for a dynamic, self-ordering system that is able to quickly remodel itself in response to external cues. Self-remodelling indeed allows treadmilling filaments to rapidly respond to external biases, such as local curvature or chemical patterning, which is not achievable in systems of static filaments. This suggests that both naturally occurring but also artificial treadmilling polymers could be a useful tool in areas such as synthetic cell development or programmable active matter. We showed that such dynamic structures are easily tunable, which should be experimentally testable, for example using microfluidic devices and chemical patterning to generate different dynamic systems.

From a biological perspective, our study gives mechanistic insights into the molecular principles of rapid assembly of sparse cytoskeletal filaments into a dense Z-ring which, at least in *Bacillus subtilis* cells [20, 22], is required to recruit the septal cell wall synthesis machinery to mid-cell and thereby initiate bacterial cell division. We found that treadmilling-driven filament alignment, in tandem with filament sensing of cell curvature, cross-linking interactions, and spatiotemporal regulation of filament polymerization kinetics, drive Z-ring condensation – the rapid self-assembly of FtsZ filaments into a dense ring at the midcell. The onset of the process occurs on a timescale that is comparable to the single monomer lifetime while the further growth and maturation of the ring take minutes, as it requires stochastic dissolution and replacement of misaligned filaments. Quantitative matching between our simulations and live cell data confirms this picture.

Even in its simplicity, the model provides structural and dynamic insights into functional FtsZ assemblies and could be applied to unanswered questions in the field of bacterial division, such as the recruitment of bacterial wall synthesis machinery to the midcell, which ultimately divides the cell into two [14, 62, 63]. The model can help investigate how the dynamics of the Z-ring affects recruitment of the synthetic machinery and ultimately the growth of the cell wall at midcell.

Beyond their biological and biomimetic relevance, treadmilling filaments belong to a distinct class of active matter, which consumes energy not for motility but for turnover. This leads to a previously underappreciated mechanism of self-organisation and response to external biases, whereby activity allows to dissolve defects and collectively organise. This mechanism can also be expected to have further implications for filament collective behaviour, such as the response to perturbations and propagation of information, which will all be important to explore in the future.

Acknowledgements We thank Ivan Palaia and members of the Šarić lab for useful discussions, and Keesiang Lim and Richard W. Wong (WPI-Nano Life Science Institute, Kanazawa University) for providing access to HS-AFM. This work was supported by the Royal Society (Grant No. UF160266; C.V.C. and A.Š.), the European Union's Horizon 2020 Research and Innovation Programme (Grant No. 802960; A.Š.), the Austrian Science Fund (FWF) StandAlone P34607 (M.L), a Wellcome Trust and Royal Society Sir Henry Dale Fellowship (Grant No. 206670/Z/17/Z; S.H. and K.D.W.).

[1] José M. Andreu. How Protein Filaments Treadmill. *Biophysical Journal*, 119(4):717–720, 2020.

[2] Albrecht Wegner. Head to Tail Poloymerization of Actin. *Journal of Molecular Biology*, (108):139–150, 1976.

[3] C. Erlenkämper and K. Kruse. Treadmilling and length distributions of active polar filaments. *Journal of Chemical Physics*, 139(16), 2013.

[4] Clare M. Waterman-Storer and E.D. Salmon. Microtubule dynamics: Treadmilling comes around again. *Current Biology*, 7(6):R369–R372, jun 1997.

[5] Dulal Panda, Herbert P. Miller, and Leslie Wilson. Rapid treadmilling of brain microtubules free of microtubule-associated proteins in vitro and its suppression by tau. *Proceedings of the National Academy of Sciences of the United States of America*, 96(22):12459–12464, 1999.

[6] Agnieszka K. Rzadzinska, Mark E. Schneider, Caroline Davies, Gavin P. Riordan, and Bechara Kachar. An actin molecular treadmill and myosins maintain stereocilia functional architecture and self-renewal. *Journal of Cell Biology*, 164(6):887–897, 2004.

[7] Jonas Denk, Lorenz Huber, Emanuel Reithmann, and Erwin Frey. Active Curved Polymers Form Vortex Patterns on Membranes. *Physical Review Letters*, 116(17):1–6, 2016.

[8] M. Reza Shaebani, Adam Wysocki, Roland G. Winkler, Gerhard Gompper, and Heiko Rieger. Computational models for active matter. *Nature Reviews Physics*, 2(4):181–199, 2020.

[9] Zuzana Dunajova, Batirtze Prats Mateu, Philipp Radler, Keesiang Lim, Philipp Velicky, Johann Georg Danzl, Richard W Wong, Jens Elgeti, Edouard Hannezo 1#, and Martin Loose. Chiral and nematic phases of flexible active filaments. *bioRxiv*, page 2022.12.15.520425, 2022.

[10] Matthew J. Footer, Jacob W.J. Kerssemakers, Julie A. Theriot, and Marileen Dogterom. Direct measurement of force generation by actin filament polymerization using an optical trap. *Proceedings of the National Academy of Sciences of the United States of America*, 104(7):2181–2186, 2007.

[11] Eva Nogales, Kenneth H. Downing, Linda A. Amos, and Jan Löwe. Tubulin and FtsZ form a distinct family of GTPases. *Nature Structural Biology*, 5(6):451–458, 1998.

[12] Martin Loose and Timothy J Mitchison. The bacterial cell division proteins FtsA and FtsZ self-organize into dynamic cytoskeletal patterns. *Nature Cell Biology*, 16(1):38–46, 2014.

[13] Diego A. Ramirez-Diaz, Daniela A. García-Soriano, Ana Raso, Jonas Mücksch, Mario Feingold, Germán Rivas, and Petra Schwille. Treadmilling analysis reveals new insights into dynamic ftsz ring architecture. *PLOS Biology*, 16(5):1–20, 05 2018.

[14] Alexandre W. Bisson-Filho, Yen-Pang Hsu, Georgia R. Squyres, Erkin Kuru, Fabai Wu, Calum Jukes, Yingjie Sun, Cees Dekker, Seamus Holden, Michael S. VanNieuwenhze, Yves V. Brun, and Ethan C. Garner. Treadmilling by ftsz filaments drives peptidoglycan synthesis and bacterial cell division. *Science*, 355(6326):739–743, 2017.

[15] Xinxing Yang, Zhixin Lyu, Amanda Miguel, Ryan McQuillen, Kerwyn Casey Huang, and Jie Xiao. GTPase activity-coupled treadmilling of the bacterial tubulin FtsZ organizes septal cell wall synthesis. *Science*, 355(6326):744–747, 2017.

[16] David E. Anderson, Frederico J. Gueiros-Filho, and Harold P. Erickson. Assembly dynamics of FtsZ rings in Bacillus subtilis and Escherichia coli and effects of FtsZ-regulating proteins. *Journal of Bacteriology*, 186(17):5775–5781, 2004.

[17] Jordan M. Barrows and Erin D. Goley. FtsZ dynamics in bacterial division: What, how, and why? *Current Opinion in Cell Biology*, 68:163–172, 2021.

[18] Ryan McQuillen and Jie Xiao. Insights into the Structure, Function, and Dynamics of the Bacterial Cytokinetic FtsZ-Ring. *Annual Review of Biophysics*, 49:309–341, 2020.

[19] Christopher R. Mahone and Erin D. Goley. Bacterial cell division at a glance. *Journal of Cell Science*, 133(7):1–7, 2020.

[20] Kevin D Whitley, Calum Jukes, Nicholas Tregidgo, Eleni Karinou, Pedro Almada, Yann Cesbron, Ricardo Henriques, Cees Dekker, and Séamus Holden. FtsZ treadmilling is essential for Z-ring condensation and septal constriction initiation in Bacillus subtilis cell division. *Nature Communications*, 12(1):2448, 2021.

[21] Lauren C. Corbin and Harold P. Erickson. A Unified Model for Treadmilling and Nucleation of Single-Stranded FtsZ Protofilaments. *Biophysical Journal*, 119(4):792–805, 2020.

[22] Georgia R. Squyres, Matthew J. Holmes, Sarah R. Barger, Betheney R. Pennycook, Joel Ryan, Victoria T. Yan, and Ethan C. Garner. Single-molecule imaging reveals that Z-ring condensation is essential for cell division in Bacillus subtilis. *Nature Microbiology*, 2021.

[23] Jan Löwe and Linda A Amos. Crystal structure of the bacterial cell-division protein FtsZ. *Nature*, 391(6663):203–206, jan 1998.

[24] Harold P Erickson, David E Anderson, and Masaki Osawa. FtsZ in bacterial cytokinesis: cytoskeleton and force generator all in one. *Microbiol Mol Biol Rev*, 74(4):504–28, 2010.

[25] James M. Wagstaff, Matthew Tsim, María A. Oliva, Alba García-Sanchez, Danguole Kureisaite-Ciziene, José Manuel Andreu, and Jan Löwe. A polymerization-associated structural switch in ftsz

that enables treadmilling of model filaments. *mBio*, 8(3):1–16, 2017.

[26] Federico M. Ruiz, Sonia Huecas, Alicia Santos-Aledo, Elena A. Prim, José M. Andreu, and Carlos Fernández-Tornero. FtsZ filament structures in different nucleotide states reveal the mechanism of assembly dynamics. *PLoS Biology*, 20(3):1–22, 2022.

[27] Shishen Du, Sebastien Pichoff, Karsten Kruse, and Joe Lutkenhaus. FtsZ filaments have the opposite kinetic polarity of microtubules. 2018.

[28] Zhuo Li, Michael J. Trimble, Yves V. Brun, and Grant J. Jensen. The structure of FtsZ filaments in vivo suggests a force-generating role in cell division. *EMBO Journal*, 26(22):4694–4708, 2007.

[29] Yaodong Chen and Harold P. Erickson. Rapid in vitro assembly dynamics and subunit turnover of FtsZ demonstrated by fluorescence resonance energy transfer. *Journal of Biological Chemistry*, 280(23):22549–22554, 2005.

[30] Sonia Huecas, Oscar Llorca, Jasminka Boskovic, Jaime Martfn-Benito, Jose Marfa Valpuesta, and Jose Manuel Andreu. Energetics and geometry of FtsZ polymers: Nucleated self-assembly of single protofilaments. *Biophysical Journal*, 94(5):1796–1806, 2008.

[31] Paulo Caldas, Mar López-Pelegrín, Daniel J.G. Pearce, Nazmi Burak Budanur, Jan Brugués, and Martin Loose. Cooperative ordering of treadmilling filaments in cytoskeletal networks of FtsZ and its crosslinker ZapA. *Nature Communications*, 10(1), 2019.

[32] Xia-qing Shi and Hugues Chaté. Self-Propelled Rods: Linking Alignment-Dominated and Repulsion-Dominated Active Matter. pages 2–6, 2018.

[33] Robert Großmann, Igor S. Aranson, and Fernando Peruani. A particle-field approach bridges phase separation and collective motion in active matter. *Nature Communications*, 11(1):1–12, 2020.

[34] Lars Onsager. the Effects of Shape on the Interaction of Colloidal Particles. *Annals of the New York Academy of Sciences*, 51(4):627–659, 1949.

[35] Broto Tjipto-Margo and Glenn T. Evans. The Onsager theory of the isotropic-nematic liquid crystal transition: Incorporation of the higher virial coefficients. *The Journal of Chemical Physics*, 93(6):4254–4265, 1990.

[36] Misha Perepelitsa, Ilya Timofeyev, Patrick Murphy, and Oleg A. Igoshin. A mean-field model for nematic alignment of self-propelled rods. 034613:1–10, 2022.

[37] Volker Schaller, Christoph Weber, Christine Semmrich, Erwin Frey, and Andreas R. Bausch. Polar patterns of driven filaments. *Nature*, 467(7311):73–77, 2010.

[38] Alfredo Sciortino and Andreas R. Bausch. Pattern formation and polarity sorting of driven actin filaments on lipid membranes. *Proceedings of the National Academy of Sciences of the United States of America*, 118(6):1–8, 2021.

[39] Gil Henkin, Stephen J. DeCamp, Daniel T.N. Chen, Tim Sanchez, and Zvonimir Dogic. Tunable dynamics of microtubule-based active isotropic gels. *Philosophical Transactions of the Royal Society A: Mathematical, Physical and Engineering Sciences*, 372(2029), 2014.

[40] Stephen J. DeCamp, Gabriel S. Redner, Aparna Baskaran, Michael F. Hagan, and Zvonimir Dogic. Orientational order of motile defects in active nematics. *Nature Materials*, 14(11):1110–1115, 2015.

[41] Ram Dixit and Richard Cyr. Encounters between dynamic cortical microtubules promote ordering of the cortical array through angle-dependent modifications of microtubule behavior. *Plant Cell*, 16(12):3274–3284, 2004.

[42] Simon H. Tindemans, Rhoda J. Hawkins, and Bela M. Mulder. Survival of the aligned: Ordering of the plant cortical microtubule array. *Physical Review Letters*, 104(5):1–4, 2010.

[43] Philipp Radler, Natalia Baranova, Paulo Caldas, Christoph Sommer, Mar López-Pelegrín, David Michalik, and Martin Loose. In vitro reconstitution of Escherichia coli divisome activation. *Nature Communications*, 13(1):1–15, 2022.

[44] Harold P. Erickson. Modeling the physics of FtsZ assembly and force generation. *Proceedings of the National Academy of Sciences of the United States of America*, 106(23):9238–9243, 2009.

[45] Biplab Ghosh and Anirban Sain. Origin of contractile force during cell division of bacteria. *Physical Review Letters*, 101(17):1–4, 2008.

[46] Tim Nierhaus, Stephen H McLaughlin, Frank Bürmann, Danguole Kureisaite-Ciziene, Sarah Maslen, Mark J Skehel, Conny WH Yu, Stefan MV Freund, Louise FH Funke, Jason W Chin, and Jan Löwe. The bacterial actin-like cell division protein ftsa forms curved antiparallel double filaments upon binding of ftsn. *bioRxiv*, 2021.

[47] Nikolay Ouzounov, Jeffrey P. Nguyen, Benjamin P. Bratton, David Jacobowitz, Zemer Gitai, and Joshua W. Shaevitz. MreB Orientation Correlates with Cell Diameter in Escherichia coli. *Biophysical Journal*, 111(5):1035–1043, 2016.

[48] Saman Hussain, Carl N. Wivagg, Piotr Szwedziak, Felix Wong, Kaitlin Schaefer, Thierry Izoré, Lars D. Renner, Matthew J. Holmes, Yingjie Sun, Alexandre W. Bisson-Filho, Suzanne Walker, Ariel Amir, Jan Löwe, and Ethan C. Garner. Mreb filaments align along greatest principal membrane curvature to orient cell wall synthesis. *eLife*, 7:1–45, 2018.

[49] Handuo Shi, David A. Quint, Gregory M. Grason, Ajay Gopinathan, and Kerwyn Casey Huang. Chiral twisting in a bacterial cytoskeletal polymer affects filament size and orientation. *Nature Communications*, 11(1):1–12, 2020.

[50] Martin Loose, Elisabeth Fischer-friedrich, Jonas Ries, Karsten Kruse, and Petra Schwille. Spatial

Regulators for Bacterial Cell Division Self-Organize. *Science (New York, N.Y.)*, 320(May):789–792, 2008.

[51] Daniela Kiekebusch, Katharine A. Michie, Lars Oliver Essen, Jan Löwe, and Martin Thanbichler. Localized Dimerization and Nucleoid Binding Drive Gradient Formation by the Bacterial Cell Division Inhibitor MipZ. *Molecular Cell*, 46(3):245–259, 2012.

[52] Senthil Arumugam, Zdeněk Petrášek, and Petra Schwille. MinCDE exploits the dynamic nature of FtsZ filaments for its spatial regulation. *Proceedings of the National Academy of Sciences of the United States of America*, 111(13), 2014.

[53] Katja Zieske and Petra Schwille. Reconstitution of self-organizing protein gradients as spatial cues in cell-free systems. *eLife*, 3:1–19, 2014.

[54] Helge Feddersen, Laeschkir Würthner, Erwin Frey, and Marc Bramkamp. Dynamics of the bacillus subtilis min system. *mBio*, 12(2), 2021.

[55] Laura Corrales-Guerrero, Wieland Steinchen, Beatrice Ramm, Jonas Mücksch, Julia Rosum, Yacine Refes, Thomas Heimerl, Gert Bange, Petra Schwille, and Martin Thanbichler. MipZ caps the plus-end of FtsZ polymers to promote their rapid disassembly. *Proceedings of the National Academy of Sciences*, 119(50):2017, dec 2022.

[56] Beatrice Ramm, Dominik Schumacher, Andrea Harms, and Tamara Heermann. A phase-separated biomolecular condensate nucleates polymerization of the tubulin homolog FtsZ to spatiotemporally regulate bacterial cell division. pages 1–38, 2022.

[57] Ling Juan Wu and Jeff Errington. Coordination of cell division and chromosome segregation by a nucleoid occlusion protein in bacillus subtilis. *Cell*, 117(7):915–925, 2004.

[58] Joe Lutkenhaus. Linking DNA replication to the Z ring. *Nature Microbiology*, 6(9):1108–1109, 2021.

[59] J. Männik and M. W. Bailey. Spatial coordination between chromosomes and cell division proteins in Escherichia coli. *Frontiers in Microbiology*, 6(MAR):1–8, 2015.

[60] Thomas G. Bernhardt and Piet A.J. De Boer. SlmA, a nucleoid-associated, FtsZ binding protein required for blocking septal ring assembly over chromosomes in E. coli. *Molecular Cell*, 18(5):555–564, 2005.

[61] Jackson Buss, Carla Coltharp, Tao Huang, Chris Pohlmeyer, Shih Chin Wang, Christine Hatem, and Jie Xiao. In vivo organization of the FtsZ-ring by ZapA and ZapB revealed by quantitative super-resolution microscopy. *Molecular Microbiology*, 89(6):1099–1120, 2013.

[62] Paula P. Navarro, Andrea Vettiger, Virly Y. Ananda, Paula Montero Llopis, Christoph Allolio, Thomas G. Bernhardt, and Luke H. Chao. Cell wall synthesis and remodelling dynamics determine division site architecture and cell shape in Escherichia coli. *Nature Microbiology*, 7(10):1621–1634, sep 2022.

[63] Jan Samuel Puls, Dominik Brajtenbach, Tanja Schneider, Ulrich Kubitscheck, and Fabian Grein. Inhibition of peptidoglycan synthesis is sufficient for total arrest of staphylococcal cell division. *Science advances*, 9(12):eade9023, mar 2023.